RESEARCH PAPER

Comparative Molecular Docking and Interaction Profiling of OXD-Deoxy Derivatives Against SARS-CoV-2 Main Protease

Madhu Sudan1, Danveer Singh Yadav2*

1: Research scholar, Department of Chemistry, Shyam Sunder Memorial (P.G.)

College Chandausi, Sambhal 244412, Uttar Pradesh, India, Affiliated with

MJPRU Bareilly 243006, Uttar Pradesh, India

Email Id: madhusudanyadav523@gmail.com

2: *Professor/Principal, Department of Chemistry, Shyam Sunder Memorial (P.G.)

College Chandausi, Sambhal 244412, Uttar Pradesh, India, Affiliated with

MJPRU Bareilly 243006, Uttar Pradesh, India

Corresponding author Email Id: danveersingh1921@gmail.com

Abstract

SARS-CoV-2 main protease (Mpro; 3CLpro) is a validated antiviral target because it mediates viral polyprotein processing required for replication. This in silico study compared five structurally related OXD-deoxy derivatives—OXD_deoxy_amino, OXD_deoxy_chloro, OXD_deoxy_core, OXD_deoxy_methyl and OXD_deoxy_phenyl—against the SARS-CoV-2 Mpro crystal structure complexed with inhibitor N3 (PDB ID: 6LU7). Docking outputs were evaluated using ranked docking scores, confidence scores and two- and three-dimensional ligand-residue interaction profiles. OXD_deoxy_phenyl showed the most favorable predicted binding, with the best docking score (−135.89) and highest confidence score (0.4299). OXD_deoxy_amino ranked second (−111.47), followed by OXD_deoxy_chloro and OXD_deoxy_core (each approximately −110.20), whereas OXD_deoxy_methyl produced the weakest top-ranked docking score (−109.57). Interaction profiling indicated that OXD_deoxy_phenyl contacted several functionally important residues, including His41, Cys145, Glu166, Met165, Asn142, Gly143, Ser144 and Gln189. The involvement of His41 and Cys145 is particularly relevant because these residues form the catalytic dyad of Mpro. Although OXD_deoxy_methyl ranked lowest by score, its contacts with Cys145, Glu166, Gly143, Ser144 and Asn142 suggest active-site relevance. Overall, OXD_deoxy_phenyl emerged as the leading derivative for further validation. These results remain preliminary computational predictions and require molecular dynamics simulation, binding free-energy estimation, ADMET screening and experimental antiviral testing before biological activity can be inferred.

Keywords: SARS-CoV-2 main protease; 6LU7; molecular docking; OXD-deoxy derivatives; protein-ligand interactions; antiviral lead discovery.

How to cite this article: Sudan M, Yadav DS. Comparative Molecular Docking and Interaction Profiling of OXD-Deoxy Derivatives Against SARS-CoV-2 Main Protease. Int J Drug Deliv Technol. 2026;16(63s):1223-1233. DOI: 10.25258/ijddt.16.63s.119

1. Introduction

The coronavirus disease 2019 pandemic created an urgent need for rapid antiviral drug discovery. Although vaccination has reduced severe disease and mortality, SARS-CoV-2 drug discovery remains scientifically relevant because viral variants continue to emerge and available antiviral options have clinical limitations. One of the most important molecular targets for anti-SARS-CoV-2 therapy is the main protease, also known as Mpro or 3CLpro. This enzyme cleaves viral polyproteins into functional non-structural proteins required for replication and transcription. Because this proteolytic step is essential to the viral life cycle, inhibition of Mpro can suppress replication at an early biochemical stage [1,2].

SARS-CoV-2 Mpro is an attractive drug target because its active-site architecture is well characterized and differs from human proteases, which may support selective inhibitor development [2]. Structurally, the enzyme contains a catalytic dyad formed by His41 and Cys145. These residues participate directly in peptide-bond cleavage in viral polyproteins [3]. Other nearby residues, including Gly143, Ser144, Asn142, His163, His164, Met165, Glu166 and Gln189, contribute to substrate recognition, binding-pocket stability and ligand accommodation. Compounds that form stable interactions with these residues may therefore represent potential starting points for Mpro inhibitor development.

The Protein Data Bank structure 6LU7 represents SARS-CoV-2 Mpro in complex with the mechanism-based inhibitor N3. This experimentally resolved

structure was among the early Mpro templates used for structure-based screening [1]. The 6LU7 structure has been widely applied to investigate the binding behavior of natural products, synthetic compounds, repurposed drugs and derivative molecules against SARS-CoV-2 Mpro [1,4]. Its availability enables docking-based prioritization before more resource-intensive experimental testing.

Molecular docking predicts the preferred orientation of a ligand within a protein binding site and estimates relative binding strength using scoring functions. In drug discovery, docking is commonly used as an early screening approach to prioritize compounds for further experimental or computational evaluation [5]. Programs such as AutoDock Vina improved docking workflows through efficient search algorithms, scoring functions and multithreading [5]. Nevertheless, docking scores should be interpreted cautiously because they approximate binding affinity rather than measure it directly. Scoring functions may incompletely capture protein flexibility, solvent effects, entropy, protonation states and dynamic ligand behavior [6].

For this reason, docking results are most informative when numerical scores are assessed together with ligand-residue interaction patterns. A favorable docking score alone does not confirm biological activity. A ligand becomes more compelling when it forms contacts within functionally important regions of the protein, especially near catalytic or substrate-recognition residues. Protein-ligand interaction profiling can identify conventional hydrogen bonds, carbon-hydrogen bonds, pi-alkyl interactions, pi-pi stacking, pi-sulfur contacts, salt bridges, hydrophobic contacts and unfavorable interactions. These features help explain why one ligand may bind more favorably than another and whether the predicted pose occupies a pharmacologically meaningful site [7].

In SARS-CoV-2 Mpro, hydrogen bonding with Gly143, Ser144, Cys145, His163, His164, Glu166 and Gln189 is frequently associated with ligand stabilization in the active pocket. Hydrophobic and aromatic interactions with Met165, His41, Phe140, Leu141, Cys145, Pro168 and His172 may further strengthen ligand anchoring. Glu166 is particularly important because it contributes to the S1 pocket and supports ligand recognition. Similarly, interactions involving Cys145 and His41 are mechanistically important because these residues constitute the catalytic dyad [2,3].

This study evaluates five OXD-deoxy derivatives docked against the SARS-CoV-2 Mpro structure 6LU7. The examined compounds were OXD_deoxy_amino, OXD_deoxy_chloro, OXD_deoxy_core, OXD_deoxy_methyl and OXD_deoxy_phenyl. The available docking-output dataset contained three-dimensional binding poses, two-dimensional ligand-residue interaction maps and ranked docking-score tables for the top 10 models of each ligand. The extracted docking data indicated that the phenyl derivative produced the strongest predicted docking score, whereas the amino, chloro, core and methyl derivatives showed lower but still favorable docking values.

The scientific value of this comparison lies in its substituent-based interpretation of structurally related molecules against a validated SARS-CoV-2 Mpro target. Small chemical modifications can alter binding affinity, ligand orientation, electronic properties, hydrophobicity and residue-contact patterns. In the present dataset, phenyl substitution appeared to improve predicted binding relative to the amino, chloro, core and methyl derivatives. This observation suggests that aromatic extension may contribute to stronger ligand stabilization within the Mpro binding region, although this interpretation requires further computational and experimental validation.

The objective of this study was to compare the predicted binding performance of five OXD-deoxy derivatives against SARS-CoV-2 Mpro using docking-score ranking and ligand-residue interaction profiling. Specifically, the study aimed to identify the best-ranked ligand, describe the major interaction patterns of each derivative, assess whether the observed contacts involved functionally important Mpro residues and recommend the most promising derivative for further validation. The study contributes to early-stage antiviral lead prioritization by providing a structured interpretation of docking outputs for OXD-deoxy derivatives against the SARS-CoV-2 Mpro target.

2. Materials and Methods

2.1 Study Design

This study was designed as a comparative in silico molecular docking evaluation of structurally related OXD-deoxy derivatives against SARS-CoV-2 Mpro. The analysis focused on docking-score ranking, confidence-score comparison and qualitative interpretation of ligand-residue interaction profiles. Molecular docking allows ligands to be positioned within the binding site of a target protein and ranked according to predicted binding performance. It is useful at the early screening stage because it can reduce the number of compounds requiring experimental testing and can identify residue-level interactions that may support biological activity [8]. In this study, docking was treated as a predictive screening method rather than a confirmatory biological assay.

2.2 Selection of Target Protein

The target protein selected for this study was SARS-CoV-2 main protease, also known as Mpro or 3CLpro. The selected structure was PDB ID 6LU7, which represents the crystal structure of SARS-CoV-2 Mpro complexed with the inhibitor N3. This structure is frequently used in docking studies because it contains a well-defined active region and provides an experimentally resolved framework for inhibitor-binding analysis.

Mpro is biologically important because it cleaves viral polyproteins into functional non-structural proteins required for viral replication and transcription. Because humans do not have closely equivalent proteases with the same cleavage specificity, SARS-CoV-2 Mpro has been widely recognized as a suitable antiviral target [9]. The catalytic site includes the His41-Cys145 dyad and these residues were considered central during interaction interpretation.

2.3 Protein Preparation

The receptor was interpreted in its docking-ready form based on the supplied docking-output dataset. In a fully reproducible workflow, the SARS-CoV-2 Mpro crystal structure would be downloaded from the Protein Data Bank in PDB format and prepared by removing crystallographic water molecules, deleting non-essential heteroatoms, separating the co-crystallized ligand when appropriate, adding polar hydrogen atoms, assigning charges and correcting missing atoms or side chains [10].

Protein preparation is critical because docking accuracy depends strongly on the chemical and structural quality of the receptor. Hydrogen atoms are commonly absent from X-ray structures but are essential for identifying hydrogen-bond donors and acceptors. Correct protonation states are also important because they influence electrostatic contacts between ligands and binding-pocket residues [11]. For SARS-CoV-2 Mpro, careful preparation of His41, Cys145, Glu166, His163, His164, Gly143, Ser144 and Gln189 is particularly important because these residues frequently contribute to ligand stabilization.

2.4 Ligand Selection and Preparation

Five OXD-deoxy derivatives were included in the comparative docking analysis: OXD_deoxy_amino, OXD_deoxy_chloro, OXD_deoxy_core, OXD_deoxy_methyl and OXD_deoxy_phenyl. These compounds represent a related chemical series with different substituent modifications. The purpose of including these derivatives was to examine whether structural substitution influenced predicted binding strength and interaction behavior within the Mpro binding pocket.

Substituent modifications can alter hydrophobicity, electronic distribution, steric compatibility, hydrogen-bonding potential and aromatic-contact formation. These changes can meaningfully influence docking score and binding orientation [12]. In a standard docking workflow, ligand structures would be drawn or imported in two-dimensional format, converted into three-dimensional conformations, geometrically optimized, assigned correct bond orders and protonation states and saved in a docking-compatible file format. Energy minimization before docking reduces unrealistic geometry and improves conformational reliability [13].

2.5 Binding-Site Definition

The docking analysis focused on the binding region represented in the 6LU7 structure. This region includes the catalytic dyad His41 and Cys145 and surrounding residues involved in ligand recognition. Residues considered during interaction interpretation included His41, Cys145, Gly143, Ser144, Asn142, His163, His164, Met165, Glu166, Gln189, Thr111, Thr292, Phe294, Asp295, Arg298 and Gln127.

The interaction maps showed that different ligands contacted different residue combinations. For example, OXD_deoxy_phenyl interacted with His41, Cys145, Glu166, Met165, Gly143, Ser144, Asn142 and Gln189, whereas OXD_deoxy_amino contacted Gln127, Arg298, Asp295, Thr111, Thr292, Phe294 and Asn151. These residue patterns were used to assess whether each ligand occupied a pharmacologically meaningful region of the protein.

2.6 Docking Procedure

The docking procedure was interpreted from the available ranked docking outputs. Each ligand was docked against SARS-CoV-2 Mpro and the top 10 predicted binding models were generated for each compound. The models were ranked according to docking score, with more negative values interpreted as stronger predicted binding under the applied scoring function.

For each ligand, the first-ranked docking model was considered the primary pose for comparative interpretation because it represented the most favorable predicted binding orientation among the top 10 models. This approach is common in docking studies, although lower-ranked poses can also be informative when they show biologically meaningful interactions [14]. The primary docking-score values extracted from the source dataset were −111.47 for OXD_deoxy_amino, −110.20 for OXD_deoxy_chloro, −110.20 for OXD_deoxy_core, −109.57 for OXD_deoxy_methyl and −135.89 for OXD_deoxy_phenyl. OXD_deoxy_phenyl therefore showed the strongest predicted binding score among the tested compounds.

2.7 Interaction Visualization and Profiling

Protein-ligand interactions were analyzed using the two-dimensional and three-dimensional interaction maps available in the docking-output dataset. The diagrams included conventional hydrogen bonds, carbon-hydrogen bonds, pi-alkyl interactions, pi-pi interactions, pi-sulfur interactions, amide-pi stacked interactions, van der Waals contacts and unfavorable contacts. These interaction categories were interpreted to clarify the molecular basis of ligand stabilization in or near the Mpro binding pocket.

Hydrogen bonds were considered important because they can improve ligand orientation and binding specificity. Hydrophobic and aromatic interactions were also considered relevant because the Mpro binding pocket contains residues that can support ligand anchoring. Interactions involving His41, Cys145, Glu166, Gly143, Ser144, Asn142, Met165 and

Gln189 were treated as especially meaningful because these residues are associated with catalytic function, substrate recognition or active-site stability [15].

Interaction maps were not interpreted solely by the number of contacts. The biological relevance of the contacted residues was also considered. For example, a ligand interacting with Cys145, His41 or Glu166 was considered more relevant than a ligand contacting only residues distant from the recognized catalytic region. This approach provides a more meaningful interpretation than docking-score ranking alone.

2.8 Docking-Score Ranking Criteria

The tested ligands were ranked primarily by their best docking scores. A more negative docking score was interpreted as stronger predicted binding. Confidence score was used as a secondary ranking criterion, with a higher confidence score considered supportive of greater pose reliability under the applied docking-scoring framework.

The final ranking was based on three criteria: the best docking score, the confidence score and the relevance of ligand-residue contacts. OXD_deoxy_phenyl was ranked as the most promising compound because it showed the most negative docking score and the highest confidence score. The other four ligands had relatively close docking values, so their comparative interpretation required closer attention to residue-contact patterns.

2.9 Data Extraction and Tabulation

Data were extracted manually from the docking-output dataset. Extracted variables included ligand name, top-ranked docking score, confidence score, ligand RMSD, major interacting residues and interaction types. Visual inspection was used to identify residues shown in the two-dimensional interaction diagrams. The docking-score tables were used to collect top-10 model summaries for each ligand and the interaction diagrams were used to describe ligand orientation and residue-contact patterns.

The extracted docking scores were arranged into comparative tables. The best-ranked pose for each ligand was used for primary analysis. Secondary poses were acknowledged but were not interpreted individually in detail because the aim of the study was to compare the best predicted binding performance of each derivative.

2.10 Methodological Limitations

Several methodological limitations were recognized. First, the study depended on docking-output figures and score tables rather than raw docking files. As a result, key reproducibility details, including grid-box dimensions, exhaustiveness, scoring-function settings, ligand protonation states, receptor-preparation parameters and docking-software settings, were not available. Second, molecular docking provides static binding predictions and does not fully represent protein and ligand dynamics under physiological conditions. Third, docking scores are not equivalent to experimentally measured binding affinities. Fourth, biological activity, toxicity, solubility, metabolic stability and cellular uptake cannot be confirmed from docking alone.

Because of these limitations, the present docking results should be interpreted as preliminary computational evidence. The best-performing ligand should be examined further using molecular dynamics simulation, MM/PBSA or MM/GBSA binding free-energy calculations, ADMET prediction, enzyme inhibition assays, cytotoxicity testing and cell-based antiviral assays [16].

3. Results

3.1 Binding Pose and Interaction Profile of 6LU7-OXD_deoxy_amino

The docking visualization for 6LU7-OXD_deoxy_amino showed that the ligand was accommodated within a residue-rich region of the SARS-CoV-2 Mpro structure (Figure 1). The three-dimensional pose indicated ligand placement within the folded protein environment, whereas the two-dimensional interaction diagrams clarified the residue-level contacts. OXD_deoxy_amino interacted with Gln127, Arg298, Asp295, Thr111, Thr292, Phe294, Asn151, Gln110, Ile106, Val104 and Phe112. The predicted interaction network included conventional hydrogen bonds, carbon-hydrogen bonds, van der Waals contacts, pi-donor hydrogen-bond interaction and pi-alkyl interaction.

Multiple polar contacts were the most notable feature of this derivative. Conventional hydrogen bonding was observed with Gln127, Asp295 and Thr111, whereas Phe294 appeared to contribute through a hydrophobic or pi-associated contact. Hydrogen bonds are important in docking interpretation because they can stabilize ligand orientation and improve binding specificity within a protein pocket [17]. The combined polar and hydrophobic contacts suggest that OXD_deoxy_amino achieved moderate stabilization through a balanced interaction pattern.

However, the interaction map did not show strong centering of this ligand on the classical catalytic dyad region of SARS-CoV-2 Mpro. His41 and Cys145 were not dominant in the displayed interaction pattern. Therefore, although the docking score was favorable, the biological relevance of the pose should be interpreted cautiously. A ligand may achieve a favorable docking score while binding away from the most functionally important catalytic region [18]. Overall, OXD_deoxy_amino showed a stable predicted pose but appeared less active-site-focused than OXD_deoxy_methyl and OXD_deoxy_phenyl.

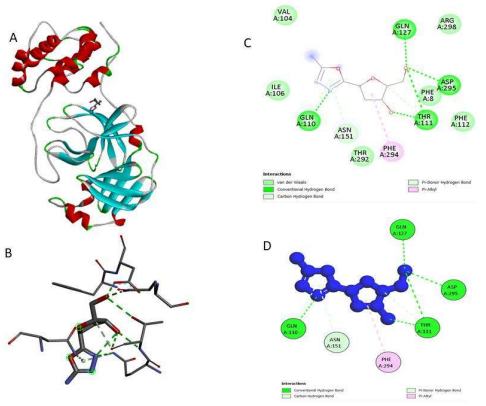

Figure 1. Predicted binding pose and two-dimensional interaction profile of OXD_deoxy_amino docked against SARS-CoV-2 Mpro (PDB ID: 6LU7). The interaction map indicates contacts with Gln127, Arg298, Asp295, Thr111, Thr292, Phe294, Asn151, Gln110, Ile106, Val104 and Phe112.

Table 1. Summary of the top 10 docking models for 6LU7-OXD_deoxy_amino.

Rank	Docking Score	Confidence Score	Ligand RMSD (Å)
1	−111.47	0.3163	66.30
2	−108.84	0.3051	73.98
3	−107.43	0.2991	67.16
4	−106.08	0.2935	65.17
5	−104.10	0.2854	73.87
6	−100.51	0.2710	68.52
7	−100.26	0.2700	58.25
8	−99.23	0.2659	50.62
9	−95.70	0.2524	52.58
10	−94.89	0.2493	58.06

3.2 Binding Pose and Interaction Profile of 6LU7-OXD_deoxy_chloro

The docking visualization for 6LU7-OXD_deoxy_chloro showed that the ligand occupied a binding region involving several residues also observed for the amino derivative (Figure 2). The ligand contacted Thr292, Asp295, Thr111, Gln127, Phe294, Asn151, Ser158, Asp153, Gln110, Phe112 and Phe8. The interaction categories included conventional hydrogen bonding, carbon-hydrogen bonding, pi-alkyl interaction, van der Waals contacts and one unfavorable bump indicated in the interaction map.

The presence of Thr111, Gln127 and Asp295 suggested that the chloro derivative formed polar contacts with the binding environment. Chloro substitution may influence ligand orientation by modifying electronic and steric properties. Halogen substitution can sometimes improve ligand binding by increasing hydrophobicity or enabling directional contacts, although these effects depend strongly on geometry and pocket compatibility [20].

A notable feature was the unfavorable interaction involving Thr111. Unfavorable contacts may reduce pose stability despite the presence of other favorable interactions. Thus, although OXD_deoxy_chloro showed a good docking score, its orientation may involve steric or electrostatic strain. Compared with OXD_deoxy_amino, the chloro derivative showed a similar interaction region but a slightly weaker best docking score. Its profile did not show strong direct involvement of His41 and Cys145, suggesting that it may not be the strongest active-site-directed candidate among the tested compounds.

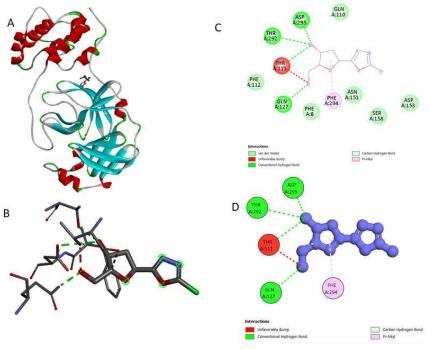

Figure 2. Predicted binding pose and two-dimensional interaction profile of OXD_deoxy_chloro docked against SARS-CoV-2 Mpro. The interaction profile shows contacts with Thr292, Asp295, Thr111, Gln127, Phe294, Asn151, Ser158, Asp153, Gln110, Phe112 and Phe8, including one unfavorable contact.

Table 2. Summary of the top 10 docking models for 6LU7-OXD_deoxy_chloro.

Rank	Docking Score	Confidence Score	Ligand RMSD (Å)
1	−110.20	0.3109	66.64
2	−106.40	0.2950	74.16
3	−105.83	0.2925	66.63
4	−103.54	0.2831	74.98
5	−103.04	0.2811	70.29
6	−95.56	0.2518	52.93
7	−91.13	0.2355	58.38
8	−91.06	0.2353	50.01
9	−90.88	0.2346	58.45
10	−90.29	0.2325	58.04

3.3 Binding Pose and Interaction Profile of 6LU7-OXD_deoxy_core

The docking visualization for 6LU7-OXD_deoxy_core showed a binding pattern broadly similar to that of the chloro derivative (Figure 3). The source table labelled this ligand as 6LU7-OXD_deoxy_coro; however, it is treated here as OXD_deoxy_core for consistency with the compound set. The interaction map showed contacts with Ile106, Gln110, Asn151, Thr111, Thr292, Asp295, Gln127, Arg298, Phe294 and Phe8.

OXD_deoxy_core formed conventional hydrogen bonds and other non-covalent contacts with surrounding residues. The interaction profile suggested stabilization by a combination of polar and hydrophobic contacts. However, the map also showed an unfavorable acceptor-acceptor type contact involving Asp295, which may reduce the favorability of that ligand orientation.

The core derivative provides a baseline scaffold for comparison with substituted analogues. Relative to the amino, chloro, methyl and phenyl derivatives, the core compound helps indicate whether substituent modification improves or weakens predicted binding. OXD_deoxy_core had a favorable docking score but did not outperform the phenyl derivative. It also did not show strong interaction with His41 or Cys145 in the displayed pose, limiting its predicted active-site relevance compared with derivatives that contacted residues closer to the catalytic region.

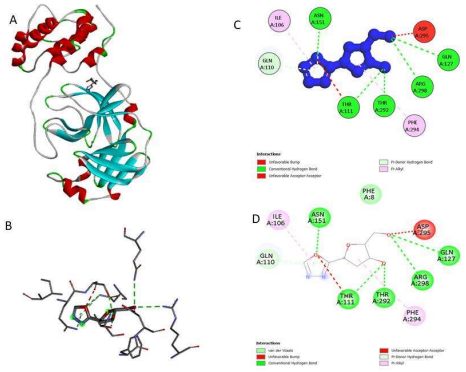

Figure 3. Predicted binding pose and two-dimensional interaction profile of OXD_deoxy_core docked against SARS-CoV-2 Mpro. The ligand contacts Ile106, Gln110, Asn151, Thr111, Thr292, Asp295, Gln127, Arg298, Phe294 and Phe8.

Table 3. Summary of the top 10 docking models for 6LU7-OXD_deoxy_core.

Rank	Docking Score	Confidence Score	Ligand RMSD (Å)
1	−110.20	0.3109	65.64
2	−106.44	0.2950	74.16
3	−105.83	0.2925	66.63
4	−103.54	0.2831	74.98
5	−103.04	0.2811	70.29
6	−95.56	0.2518	52.93
7	−91.13	0.2355	58.38
8	−91.06	0.2353	50.01
9	−90.88	0.2346	58.45
10	−90.29	0.2325	58.04

3.4 Binding Pose and Interaction Profile of 6LU7-OXD_deoxy_methyl

The docking visualization for 6LU7-OXD_deoxy_methyl showed a more active-site-relevant interaction profile than the amino, chloro and core derivatives (Figure 4). The ligand contacted residues near the recognized SARS-CoV-2 Mpro active region, including Cys145, Glu166, His163, His164, Asn142, Ser144, Gly143, Met165, Phe140, His172 and Leu141. These residues are commonly associated with ligand binding in the Mpro active pocket.

Cys145 is particularly important because it forms part of the catalytic dyad with His41. Although His41 was not dominant in the methyl derivative interaction figure, contact with Cys145 suggests that the ligand may be positioned near a functionally important region of the protease. The involvement of Glu166 is also relevant because this residue helps shape the S1 pocket and stabilize ligand recognition. Contacts with Gly143, Ser144 and Asn142 further suggest proximity to the oxyanion-hole region, which is important for substrate recognition and catalytic-site stabilization.

The interaction types included conventional hydrogen bonding, carbon-hydrogen bonding, pi-anion interaction, amide-pi stacked interaction, alkyl interaction, pi-alkyl interaction and van der Waals contacts. The methyl group likely contributed to hydrophobic contacts, whereas the remaining ligand scaffold supported polar interactions with active-site residues. Despite this biologically relevant interaction profile, the docking score of OXD_deoxy_methyl was slightly weaker than those of the amino, chloro and core derivatives. This finding indicates that residue relevance and numerical docking score did not rank the compound identically.

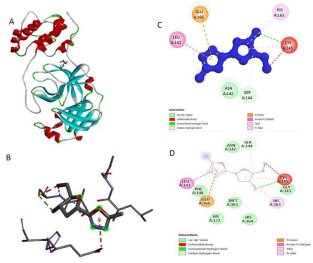

Figure 4. Predicted binding pose and two-dimensional interaction profile of OXD_deoxy_methyl docked against SARS-CoV-2 Mpro. The ligand contacts active-site-associated residues, including Cys145,

Glu166, His163, His164, Asn142, Ser144, Gly143, Met165, Phe140, His172 and Leu141.

Table 4. Summary of the top 10 docking models for 6LU7-OXD_deoxy_methyl.

Rank	Docking Score	Confidence Score	Ligand RMSD (Å)
1	−109.57	0.3082	66.30
2	−107.05	0.2975	74.79
3	−107.04	0.2975	66.24
4	−105.57	0.2914	69.84
5	−101.81	0.2761	73.60
6	−100.80	0.2721	66.83
7	−96.70	0.2562	51.63
8	−93.23	0.2432	75.34
9	−92.58	0.2408	73.47
10	−91.98	0.2386	57.57

3.5 Binding Pose and Interaction Profile of 6LU7-OXD_deoxy_phenyl

The docking visualization for 6LU7-OXD_deoxy_phenyl showed the most favorable overall interaction profile among the tested derivatives (Figure 5). The compound formed contacts with several functionally important residues, including His41, Cys145, Glu166, Met165, Asn142, Gly143, Ser144, His163, His172, Leu141, Phe140, Met49, Gln189, Arg188 and Asp187. These residues are located within or close to the recognized binding pocket of SARS-CoV-2 Mpro.

The presence of both His41 and Cys145 is highly relevant because these residues form the catalytic dyad of SARS-CoV-2 Mpro. A compound predicted to bind near these residues may have a greater chance of interfering with catalytic activity than a ligand predicted to bind away from the catalytic region. Interactions with Glu166, Gly143, Ser144 and Asn142 further suggest that OXD_deoxy_phenyl was positioned near residues involved in substrate recognition and active-site stabilization.

The interaction map showed several non-covalent interaction types, including carbon-hydrogen bonding, pi-sulfur interaction, pi-pi stacked interaction, alkyl interaction, pi-alkyl interaction and van der Waals contacts. The phenyl substituent likely contributed to aromatic and hydrophobic stabilization, which may explain why OXD_deoxy_phenyl produced a substantially stronger docking score than the other derivatives. Compared with the other four ligands, OXD_deoxy_phenyl showed the best combination of docking strength and active-site interaction relevance.

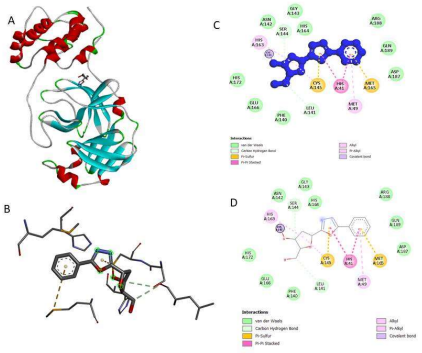

Figure 5. Predicted binding pose and two-dimensional interaction profile of OXD_deoxy_phenyl docked against SARS-CoV-2 Mpro. The ligand contacts His41, Cys145, Glu166, Met165, Asn142, Gly143, Ser144, His163, His172, Leu141, Phe140, Met49, Gln189, Arg188 and Asp187.

Table 5. Summary of the top 10 docking models for 6LU7-OXD_deoxy_phenyl.

Rank	Docking Score	Confidence Score	Ligand RMSD (Å)
1	−135.89	0.4299	70.76
2	−130.80	0.4052	72.01
3	−121.57	0.3616	65.32
4	−118.97	0.3496	73.66
5	−117.19	0.3416	66.53
6	−116.55	0.3387	67.47
7	−111.91	0.3183	65.07
8	−111.33	0.3157	66.78
9	−109.52	0.3080	50.61
10	−108.09	0.3019	67.52

3.6 Overall Ranking of the Tested OXD-Deoxy Derivatives

Based on the best docking scores, confidence scores and residue-contact relevance, the overall ranking identified OXD_deoxy_phenyl as the leading compound among the five derivatives (Table 6). It showed the best docking score, highest confidence score and strongest active-site interaction profile. Although OXD_deoxy_methyl showed the weakest numerical docking score, its contact pattern was biologically meaningful because it involved Cys145, Glu166, Gly143, Ser144 and Asn142. Therefore, OXD_deoxy_phenyl should be prioritized as the main candidate for further validation, whereas OXD_deoxy_methyl may be retained as a secondary active-site-focused candidate.

Table 6. Overall ranking of the tested OXD-deoxy derivatives based on best docking score, confidence score and interaction relevance.

Overall Rank	Ligand	Best Docking Score	Confidence Score	Interpretation
1	OXD_deoxy_phenyl	−135.89	0.4299	Strongest predicted binder
2	OXD_deoxy_amino	−111.47	0.3163	Second-best docking score
3	OXD_deoxy_chloro	−110.20	0.3109	Moderate predicted binding
4	OXD_deoxy_core	−110.20	0.3109	Comparable to the chloro derivative
5	OXD_deoxy_methyl	−109.57	0.3082	Weakest score but active-site-relevant contacts

To consolidate the ligand-specific outputs, an integrated results dashboard was prepared and placed after the overall ranking table (Figure 6). This placement allows the numerical hierarchy and the representative interaction maps to be interpreted together after all individual ligand profiles have been presented. The dashboard summarizes the stronger score and confidence profile of OXD_deoxy_phenyl and the active-site-relevant interaction pattern of OXD_deoxy_methyl without introducing additional computational or experimental values.

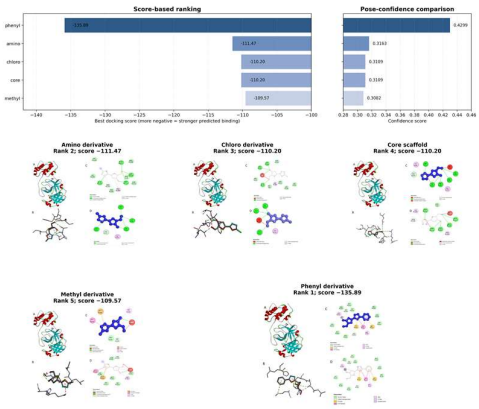

Figure 6. Integrated results dashboard showing the comparative best docking scores, confidence scores and representative ligand-interaction figures for all five OXD-deoxy derivatives. The dashboard summarizes the source docking outputs and should be interpreted as a visual synthesis of the reported results rather than as an additional experimental dataset.

4. Discussion

This docking analysis compared five OXD-deoxy derivatives against SARS-CoV-2 Mpro using the 6LU7 structure. The tested compounds showed clear variation in docking-score performance, confidence score and residue-level interaction profiles. OXD_deoxy_phenyl demonstrated the strongest predicted binding, with a best docking score of −135.89 and a confidence score of 0.4299. This score was notably stronger than those of the remaining derivatives, whose best docking scores ranged from −111.47 to −109.57. The phenyl derivative also maintained favorable scores across multiple ranked poses, suggesting that its predicted binding was not limited to a single isolated orientation.

The superior docking performance of OXD_deoxy_phenyl may be explained by its broader interaction network and the presence of aromatic and hydrophobic contacts. The phenyl group can increase hydrophobic surface area and support pi-based interactions with compatible residues in the binding pocket. Aromatic groups are often useful in medicinal chemistry because they can strengthen binding through pi-pi stacking, pi-alkyl interactions and hydrophobic packing when the protein pocket provides an appropriate environment [21]. In the present study, OXD_deoxy_phenyl contacted His41, Cys145, Glu166, Met165, Asn142, Gly143, Ser144, His163, His172, Leu141, Phe140, Met49, Gln189, Arg188 and Asp187. This interaction pattern was more active-site-relevant than those observed for several other derivatives.

OXD_deoxy_amino, OXD_deoxy_chloro, OXD_deoxy_core and OXD_deoxy_methyl showed relatively close docking scores. OXD_deoxy_amino had the second-best score, followed by OXD_deoxy_chloro and OXD_deoxy_core, whereas OXD_deoxy_methyl produced the weakest top-ranked score. However, numerical ranking alone did not fully reflect biological relevance. OXD_deoxy_methyl interacted with important active-site residues, including Cys145, Glu166, Gly143, Ser144, Asn142, His163, His164 and Met165. These residues are frequently discussed in SARS-CoV-2 Mpro inhibition studies because they are positioned within or near the catalytic and substrate-binding environment [22].

Two conclusions can therefore be drawn from the comparative results. First, OXD_deoxy_phenyl is the strongest overall candidate because it combines the best docking score with a biologically meaningful interaction profile. Second, OXD_deoxy_methyl should not be dismissed solely because of its weaker score, since it contacts several key active-pocket residues. Docking studies are most reliable when binding scores are interpreted alongside interaction

biology because scoring functions can overestimate or underestimate the importance of specific poses [23].

The catalytic dyad of SARS-CoV-2 Mpro, formed by His41 and Cys145, is central to the proteolytic mechanism. A ligand predicted to bind near this dyad may interfere with substrate access, catalytic geometry or local pocket stability. In this study, OXD_deoxy_phenyl showed proximity to both His41 and Cys145, whereas OXD_deoxy_methyl clearly contacted Cys145. The phenyl derivative is therefore particularly important because its predicted pose appears to occupy a region closely associated with catalytic function.

Other residues, including Gly143, Ser144, Asn142, His163, His164, Met165, Glu166 and Gln189, also contribute to the Mpro substrate-binding region. Gly143, Ser144 and Cys145 are associated with the oxyanion-hole region, which helps stabilize reaction intermediates during proteolysis. Glu166 is important for shaping the S1 pocket and supporting ligand recognition, whereas Met165 and Gln189 contribute to pocket flexibility and ligand accommodation [24]. The presence of these residues in the interaction profiles of OXD_deoxy_phenyl and OXD_deoxy_methyl strengthens the interpretation that these compounds may bind in pharmacologically meaningful regions.

By contrast, OXD_deoxy_amino, OXD_deoxy_chloro and OXD_deoxy_core showed favorable docking scores but their major contacts appeared more associated with Gln127, Arg298, Asp295, Thr111, Thr292, Phe294 and Asn151. These contacts may contribute to ligand binding but they are less directly connected to the classical catalytic pocket than the interactions observed for the phenyl and methyl derivatives. Their biological importance would require further confirmation, especially if these regions are proposed to influence Mpro activity allosterically.

The tested compounds also provide a preliminary structure-activity interpretation. The core derivative served as a baseline scaffold, whereas the amino, chloro, methyl and phenyl derivatives introduced modifications that changed polarity, hydrophobicity, steric bulk and aromatic character. The amino derivative produced the second-best docking score, likely reflecting its ability to form polar contacts and hydrogen bonds. However, its interaction pattern did not strongly involve the catalytic dyad, reducing its priority as a direct active-site candidate.

The chloro derivative showed a docking score similar to the core derivative. Chlorine substitution can sometimes improve binding by increasing hydrophobicity or forming halogen-related contacts [20]. In the present dataset, however, chloro substitution did not substantially improve predicted docking performance relative to the core scaffold. An unfavorable contact observed in the interaction map may partly explain why this derivative did not exceed the amino or phenyl derivatives.

The methyl derivative produced the weakest docking score but one of the more relevant active-site interaction profiles. Methyl groups are small hydrophobic substituents that can improve pocket filling and hydrophobic contact without greatly increasing molecular size. In this case, OXD_deoxy_methyl interacted with Cys145, Glu166, Gly143, Ser144, Asn142, Met165, His163 and His164. This suggests that the methyl derivative may have adopted a biologically meaningful pose even though its predicted binding strength was lower than that of the other derivatives.

The phenyl derivative showed the most convincing improvement. Its aromatic substituent likely enhanced hydrophobic and pi-based stabilization within the protein pocket. The phenyl group may also have increased interaction opportunities with His41, Met49, Cys145, Met165 and His172. This result supports the possibility that aromatic extension of the OXD-deoxy scaffold improves predicted binding against SARS-CoV-2 Mpro. Nevertheless, this conclusion remains preliminary because docking does not directly measure inhibition, solubility, permeability or toxicity.

The present findings are consistent with earlier docking-based studies showing that strong Mpro inhibitors often interact with His41, Cys145, Glu166, Gly143, Ser144, Met165 and Gln189. Many reported Mpro inhibitors stabilize the active site through a combination of hydrogen bonds, hydrophobic contacts and aromatic interactions. These interactions may position a ligand to block substrate access or disturb catalytic function [25]. The involvement of Glu166 and Cys145 in the phenyl and methyl derivatives supports their selection for further validation.

The main pharmacological implication is that OXD_deoxy_phenyl may serve as a promising starting point for further antiviral lead optimization. Its strong docking score and active-site interaction profile suggest more favorable predicted binding to SARS-CoV-2 Mpro than the other tested derivatives. If future simulations and experimental assays confirm stable binding and enzyme inhibition, the phenyl derivative could be considered for further structural optimization. However, docking-based prediction is only an early stage of drug discovery. A candidate must also demonstrate stable binding under dynamic conditions, favorable binding free energy, acceptable solubility, suitable permeability, low toxicity, metabolic stability and measurable antiviral activity.

The study has several limitations that should temper interpretation. The analysis was based on docking-output figures and score tables rather than raw docking files. Important computational details, including docking software, grid-box dimensions, exhaustiveness settings, ligand protonation states, receptor-preparation protocol, charge assignment and redocking validation, were not available. These details are essential for full methodological reproducibility and will likely be requested during peer review. Docking also provides a

static approximation of binding, whereas proteins and ligands are flexible under physiological conditions. Molecular dynamics simulations would be needed to determine whether the predicted poses remain stable over time using metrics such as root mean square deviation, root mean square fluctuation, radius of gyration, hydrogen-bond occupancy, solvent-accessible surface area and binding free-energy estimates [26].

Finally, docking scores are not experimental binding affinities. A more negative docking score does not necessarily indicate stronger biological inhibition. Scoring functions simplify complex interactions and may not fully account for structured water molecules, entropy, induced fit, desolvation penalties or conformational change. No ADMET, toxicity or experimental antiviral evaluation was included in the available output. Therefore, the present study should be interpreted as a lead-prioritization exercise rather than evidence of antiviral efficacy.

5. Conclusions

This in silico study compared five OXD-deoxy derivatives against SARS-CoV-2 Mpro using docking-score ranking and protein-ligand interaction profiling. OXD_deoxy_phenyl emerged as the leading derivative, producing the strongest docking score (−135.89), the highest confidence score (0.4299) and a broad interaction profile involving key active-site residues, including His41, Cys145, Glu166, Met165, Gly143, Ser144, Asn142, His163 and Gln189.

OXD_deoxy_amino ranked second by docking score, whereas OXD_deoxy_chloro and OXD_deoxy_core showed similar moderate predicted binding. OXD_deoxy_methyl had the weakest docking score but displayed meaningful active-site contacts, particularly with Cys145, Glu166, Gly143, Ser144 and Asn142. The overall ranking therefore supports OXD_deoxy_phenyl as the principal derivative for further investigation, while OXD_deoxy_methyl may remain useful for active-site-focused optimization.

The findings suggest that phenyl substitution may improve the predicted binding performance of the OXD-deoxy scaffold against SARS-CoV-2 Mpro. However, the evidence remains computational and preliminary. Molecular dynamics simulation, MM/PBSA or MM/GBSA free-energy calculation, ADMET screening, enzyme inhibition assays and antiviral cell-culture studies are required before biological or therapeutic claims can be made.

References

[1] Jin, Z.; Du, X.; Xu, Y.; Deng, Y.; Liu, M.; Zhao, Y.; Zhang, B.; Li, X.; Zhang, L.; Peng, C.; Duan, Y.; Yu, J.; Wang, L.; Yang, K.; Liu, F.; Jiang, R.; Yang, X.; You, T.; Liu, X.; et al. Structure of Mpro from SARS-CoV-2 and Discovery of Its Inhibitors. Nature 2020, 582(7811), 289-293. https://doi.org/10.1038/s41586-020-2223-y

[2] Ullrich, S.; Nitsche, C. The SARS-CoV-2 Main Protease as Drug Target. Bioorganic & Medicinal Chemistry Letters 2020, 30(17), 127377. https://doi.org/10.1016/j.bmcl.2020.127377

[3] Ferreira, J. C.; Fadl, S.; Villanueva, A. J.; Rabeh, W. M. Catalytic Dyad Residues His41 and Cys145 Impact the Catalytic Activity and Overall Conformational Fold of the Main SARS-CoV-2 Protease 3-Chymotrypsin-like Protease. Frontiers in Chemistry 2021, 9, 692168. https://doi.org/10.3389/fchem.2021.692168

[4] RCSB Protein Data Bank. 6LU7: The Crystal Structure of COVID-19 Main Protease in Complex with an Inhibitor N3. RCSB PDB, 2020.

[5] Trott, O.; Olson, A. J. AutoDock Vina: Improving the Speed and Accuracy of Docking with a New Scoring Function, Efficient Optimization and Multithreading. Journal of Computational Chemistry 2010, 31(2), 455-461. https://doi.org/10.1002/jcc.21334

[6] Guedes, I. A.; Pereira, F. S. S.; Dardenne, L. E. New Machine Learning and Physics-Based Scoring Functions for Drug Discovery. Scientific Reports 2021, 11, 3198. https://doi.org/10.1038/s41598-021-82410-1

[7] Salentin, S.; Schreiber, S.; Haupt, V. J.; Adasme, M. F.; Schroeder, M. PLIP: Fully Automated Protein-Ligand Interaction Profiler. Nucleic Acids Research 2015, 43(W1), W443-W447. https://doi.org/10.1093/nar/gkv315

[8] Meng, X. Y.; Zhang, H. X.; Mezei, M.; Cui, M. Molecular Docking: A Powerful Approach for Structure-Based Drug Discovery. Current Computer-Aided Drug Design 2011, 7(2), 146-157. https://doi.org/10.2174/157340911795677602

[9] Anand, K.; Ziebuhr, J.; Wadhwani, P.; Mesters, J. R.; Hilgenfeld, R. Coronavirus Main Proteinase 3CLpro Structure: Basis for Design of Anti-SARS Drugs. Science 2003, 300(5626), 1763-1767. https://doi.org/10.1126/science.1085658

[10] Sastry, G. M.; Adzhigirey, M.; Day, T.; Annabhimoju, R.; Sherman, W. Protein and Ligand Preparation: Parameters, Protocols and Influence on Virtual Screening Enrichments. Journal of Computer-Aided Molecular Design 2013, 27(3), 221-234. https://doi.org/10.1007/s10822-013-9644-8

[11] Olsson, M. H. M.; Søndergaard, C. R.; Rostkowski, M.; Jensen, J. H. PROPKA3: Consistent Treatment of Internal and Surface Residues in Empirical pKa Predictions. Journal of Chemical Theory and Computation 2011, 7(2), 525-537. https://doi.org/10.1021/ct100578z

[12] Patrick, G. L. An Introduction to Medicinal Chemistry, 6th ed.; Oxford University Press: Oxford, UK, 2017.

[13] Halgren, T. A. Merck Molecular Force Field. I. Basis, Form, Scope, Parameterization and Performance of MMFF94. Journal of Computational Chemistry 1996, 17(5-6), 490-519. https://doi.org/10.1002/(SICI)1096-987X(199604)17:5/6%3C490::AID-JCC1%3E3.0.CO;2-P

[14] Morris, G. M.; Huey, R.; Lindstrom, W.; Sanner, M. F.; Belew, R. K.; Goodsell, D. S.; Olson, A. J. AutoDock4 and AutoDockTools4: Automated Docking with Selective Receptor Flexibility. Journal of Computational Chemistry 2009, 30(16), 2785-2791. https://doi.org/10.1002/jcc.21256

[15] de Ruyck, J.; Brysbaert, G.; Blossey, R.; Lensink, M. F. Molecular Docking as a Popular Tool in Drug Design, an In Silico Travel. Advances and Applications in Bioinformatics and Chemistry 2016, 9, 1-11. https://doi.org/10.2147/AABC.S105289

[16] Genheden, S.; Ryde, U. The MM/PBSA and MM/GBSA Methods to Estimate Ligand-Binding Affinities. Expert Opinion on Drug Discovery 2015, 10(5), 449-461. https://doi.org/10.1517/17460441.2015.1032936

[17] Laskowski, R. A.; Swindells, M. B. LigPlot+: Multiple Ligand-Protein Interaction Diagrams for Drug Discovery. Journal of Chemical Information and Modeling 2011, 51(10), 2778-2786. https://doi.org/10.1021/ci200227u

[18] Wallace, A. C.; Laskowski, R. A.; Thornton, J. M. LIGPLOT: A Program to Generate Schematic Diagrams of Protein-Ligand Interactions. Protein Engineering, Design and Selection 1995, 8(2), 127-134. https://doi.org/10.1093/protein/8.2.127

[19] Kitchen, D. B.; Decornez, H.; Furr, J. R.; Bajorath, J. Docking and Scoring in Virtual Screening for Drug Discovery: Methods and Applications. Nature Reviews Drug Discovery 2004, 3(11), 935-949. https://doi.org/10.1038/nrd1549

[20] Matter, H.; Nazaré, M.; Güssregen, S.; Will, D. W.; Schreuder, H.; Bauer, A.; Urmann, M.; Ritter, K.; Wagner, M.; Wehner, V. Evidence for C-Cl/C-Br···pi Interactions as an Important Contribution to Protein-Ligand Binding Affinity. Angewandte Chemie International Edition 2009, 48(16), 2911-2916. https://doi.org/10.1002/anie.200806219

[21] Böhm, H. J.; Flohr, A.; Stahl, M. Scaffold Hopping. Drug Discovery Today: Technologies 2004, 1(3), 217-224. https://doi.org/10.1016/j.ddtec.2004.10.009

[22] Zhang, L.; Lin, D.; Sun, X.; Curth, U.; Drosten, C.; Sauerhering, L.; Becker, S.; Rox, K.; Hilgenfeld, R. Crystal Structure of SARS-CoV-2 Main Protease Provides a Basis for Design of Improved alpha-Ketoamide Inhibitors. Science 2020, 368(6489), 409-412. https://doi.org/10.1126/science.abb3405

[23] Warren, G. L.; Andrews, C. W.; Capelli, A. M.; Clarke, B.; LaLonde, J.; Lambert, M. H.; Lindvall, M.; Nevins, N.; Semus, S. F.; Senger, S.; Tedesco, G.; Wall, I. D.; Woolven, J. M.; Peishoff, C. E.; Head, M. S. A Critical Assessment of Docking Programs and Scoring Functions. Journal of Medicinal Chemistry 2006, 49(20), 5912-5931. https://doi.org/10.1021/jm050362n

[24] Kneller, D. W.; Phillips, G.; O'Neill, H. M.; Jedrzejczak, R.; Stols, L.; Langan, P.; Joachimiak, A.; Coates, L.; Kovalevsky, A. Structural Plasticity of SARS-CoV-2 3CL Mpro Active Site Cavity Revealed by Room-Temperature X-ray Crystallography. Nature Communications 2020, 11, 3202. https://doi.org/10.1038/s41467-020-16954-7

[25] Dai, W.; Zhang, B.; Jiang, X. M.; Su, H.; Li, J.; Zhao, Y.; Xie, X.; Jin, Z.; Peng, J.; Liu, F.; Li, C.; Li, Y.; Bai, F.; Wang, H.; Cheng, X.; Cen, X.; Hu, S.; Yang, X.; Wang, J.; et al. Structure-Based Design of Antiviral Drug Candidates Targeting the SARS-CoV-2 Main Protease. Science 2020, 368(6497), 1331-1335. https://doi.org/10.1126/science.abb4489

[26] Hollingsworth, S. A.; Dror, R. O. Molecular Dynamics Simulation for All. Neuron 2018, 99(6), 1129-1143. https://doi.org/10.1016/j.neuron.2018.08.011